

# Highlights from the NA60 experiment

Alessandro De Falco for the NA60 Collaboration

R Arnaldi<sup>a</sup>, K Banicz<sup>c e</sup>, K Borer<sup>d</sup>, J Castor<sup>f</sup>, B Chaurand<sup>g</sup>,  
 W Chen<sup>h</sup>, C Cicalo<sup>j</sup>, A Colla<sup>b a</sup>, P Cortese<sup>b</sup>, S Damjanovic<sup>c e</sup>,  
 A David<sup>e n</sup>, A de Falco<sup>k j</sup>, A Devaux<sup>f</sup>, L Ducroux<sup>i</sup>, H En'yo<sup>l</sup>,  
 J Fargeix<sup>g</sup>, A Ferretti<sup>b a</sup>, M Floris<sup>k j</sup>, P Force<sup>f</sup>, A Forster<sup>e</sup>,  
 N Guettet<sup>e f</sup>, A Guichard<sup>i</sup>, H Gulkanian<sup>m</sup>, J Heuser<sup>l</sup>,  
 M Keil<sup>e n</sup>, L Kluberg<sup>g</sup>, Z Li<sup>h</sup>, C Lourenço<sup>e</sup>, J Lozano<sup>n</sup>,  
 F Manso<sup>f</sup>, P Martins<sup>e n</sup>, A Masoni<sup>j</sup>, A Neves<sup>n</sup>, H Ohnishi<sup>l</sup>,  
 C Oppedisano<sup>b a</sup>, P Parracho<sup>e n</sup>, P Pillot<sup>i</sup>, T. Poghosyan<sup>m</sup>,  
 G Puddu<sup>k j</sup>, E Radermacher<sup>e</sup>, P Ramalhte<sup>e n</sup>, P Rosinsky<sup>e</sup>,  
 E Scomparin<sup>a</sup>, J Seixas<sup>n</sup>, S Serici<sup>k j</sup>, R Shahoyan<sup>n</sup>,  
 P Sonderegger<sup>e n</sup>, H J Specht<sup>c</sup>, R Tieulent<sup>i</sup>, G Usai<sup>k j</sup>,  
 R Veenhof<sup>e</sup>, H Wöhri<sup>j n</sup>

<sup>a</sup>INFN Torino, Italy

<sup>b</sup>Università di Torino, Italy

<sup>c</sup>Physikalisches Institut der Universität Heidelberg, Germany

<sup>d</sup>Laboratory for High Energy Physics, University of Bern, Bern, Switzerland

<sup>e</sup>CERN, 1211 Geneva 23, Switzerland

<sup>f</sup>LPC, Université Blaise Pascal and CNRS-IN2P3, Clermont-Ferrand, France

<sup>g</sup>LLR, Ecole Polytechnique and CNRS-IN2P3, Palaiseau, France

<sup>h</sup>Brookhaven National Laboratory, Upton, New York, USA

<sup>i</sup>IPN-Lyon, Université Claude Bernard Lyon-I and CNRS-IN2P3, Lyon, France

<sup>j</sup>INFN Cagliari, Italy

<sup>k</sup>Università di Cagliari, Italy

<sup>l</sup>RIKEN, Wako, Saitama, Japan

<sup>m</sup>YerPhI, Yerevan Physics Institute, Yerevan, Armenia

<sup>n</sup>Instituto Superior Técnico, Lisbon, Portugal

E-mail: [alessandro.de.falco@ca.infn.it](mailto:alessandro.de.falco@ca.infn.it)

**Abstract.** NA60 measured dimuon production in p-A and In-In collisions at the CERN SPS. This paper presents a high statistics measurement of  $\phi$  meson production in In-In collisions at 158 AGeV. Both the transverse momentum, rapidity, decay angular distributions and the absolute yield were measured as a function of centrality. The results are compared to previous measurements in order to shed light on the long standing  $\phi$  puzzle. In addition, highlights on  $\eta$  meson production and on the dimuon excess below the  $J/\psi$  mass are presented.

## 1. Introduction

Lepton pairs production is particularly suitable as a probe of the hot and dense medium created in high-energy heavy ion collisions, because they can access several Quark-Gluon Plasma (QGP) signatures. Among them is strangeness enhancement [1] that can be addressed by measuring the  $\phi$  and  $\eta$  mesons production. The production of thermal dileptons [2], that can be detected in the intermediate mass region (IMR) between the  $\phi$  and the  $J/\psi$  peaks, is another key observable.

NA60 is an SPS third generation experiment designed to study muon pairs production with high precision and statistics. In the following, after a short description of the experimental apparatus, key results on  $\phi$  and  $\eta$  production and on the excess in the intermediate mass region will be discussed.

## 2. NA60 Detector and data selection

NA60, a fixed target experiment at the CERN SPS, is mainly dedicated to the detection of muon pairs. The apparatus and data selection procedure are fully described in [3]. The key detectors are the muon spectrometer (MS) and the vertex tracker (VT). The MS detects the muon tracks in the rapidity range  $3 < y < 4$ , and is preceded by a  $12 \lambda_I$  thick hadron absorber. The vertex tracker is a Si pixel detector placed between the target and the absorber in a 2.5 T dipole field, that tracks the muons, among the other tracks, before they suffer multiple scattering and energy loss. The muons detected in the MS are matched to the VT tracks both in momentum and angle, thus improving the mass resolution and making it possible to measure the distance between the primary vertex and the track impact point.

The sample used for the results presented in this paper was collected with a 158 A·GeV In beam impinging on a segmented In target.  $2.3 \cdot 10^8$  triggers were acquired. In order to avoid events with reinteractions of nuclear fragments in the subsequent targets, only events with one vertex in the target region were selected. The combinatorial background was evaluated by means of the event mixing technique, with an accuracy of  $\sim 1\%$  over the full dimuon mass spectrum. The contribution due to the incorrect match between the VT tracks and the muons detected in the MS was estimated either with an overlay Monte Carlo simulation or with a mixing technique. The former consists in generating a dimuon on top of a real event, while the latter mixes the MS muons of a given event with the VT tracks of another event. The two methods agree within 5%. The final sample consist of 440000 signal muon pairs, with an average signal to background ratio of about 1/7.

## 3. $\phi$ production in In-In collisions

NA60 can detect the  $\phi$  meson via its decay into both muon and kaon pairs, thus helping understanding the so-called  $\phi$  puzzle. This takes its origin from the discrepancies

observed in the  $\phi$  measurements performed by NA50 [4] in the muon channel and by NA49 [5] in the kaon channel, both in Pb-Pb collisions at 158 A-GeV. The multiplicity measured by NA50 is much higher than the one obtained by NA49. Also the inverse slopes  $T_{eff}$  of the transverse mass distributions differ: NA50 finds a value of about 230 MeV, almost independent on centrality, while NA49 measures values increasing with the number of participants  $N_{part}$  from  $\sim 250$  MeV to  $\sim 300$  MeV. It has to be stressed that the acceptance of NA50 is limited to  $p_T > 1.1$  GeV/ $c$ , while NA49 is dominated by low transverse momenta: in presence of radial flow, the measured  $T_{eff}$  will depend on the fit range, being lower at high  $p_T$ .

The origin of this discrepancy has been longely discussed. It was suggested that kaons may suffer rescattering and absorption in the medium, resulting in a depletion of kaon pairs, especially at low  $p_T$ , that leads to a reduced yield and a hardening of the  $p_T$  distribution in the hadronic channel [6]. Recent results by CERES [7] both in the hadronic and leptonic channels confirm the NA49 results, and thus suggests that there is no  $\phi$  puzzle. However, the results in dielectrons, being affected by a large error bar, are not conclusive.

NA60 measures the  $\phi$  yield in the muon channel by counting the events in the mass window  $0.98 < M_{\mu\mu} < 1.06$  GeV/ $c^2$  [8]. The signal/background ratio below the  $\phi$  peak is  $\sim 1/3$ , integrated over centrality. To account for the continuum under the  $\phi$  peak, two side windows between  $0.88 < M_{\mu\mu} < 0.92$  GeV/ $c^2$  and  $1.12 < M_{\mu\mu} < 1.16$  GeV/ $c^2$  are subtracted to the  $\phi$  window. By performing the measurement in several  $p_T$ , rapidity and decay angle intervals, raw differential distributions are extracted. They are then corrected for the acceptance using an overlay Monte Carlo tuned iteratively such that the resulting distributions reproduce the measured data. The systematic error is evaluated by varying the analysis parameters and selections. The measurement is performed for 5 centrality bins, corresponding to  $\langle N_{part} \rangle = 15, 39, 75, 132, 183$ .

The rapidity distribution, integrated over centrality, is fitted with a gaussian, giving a width  $\sigma = 1.13 \pm 0.06 \pm 0.05$ . No centrality dependence is observed. The result is in agreement with the NA49 results on several colliding systems [5],[9]. The decay angle distribution is obtained for several reference systems (Helicity, Collins-Soper, Gottfried-Jackson) resulting flat in all the cases, independent of centrality.

The transverse mass distributions, shown in fig. 1 (left) for 5 centrality bins, are fitted with the function  $1/m_T dN/dm_T = N_0 \exp(-m_T/T_{eff})$ . The resulting inverse slopes are plotted as a function of  $N_{part}$  in fig. 1 (right), showing an increase from peripheral to mid-central collisions and a saturation for most central collisions. Since in presence of radial flow the  $T_{eff}$  value may depend on the fit range, in order to compare our results with NA49 and NA50, the fit is also performed for  $p_T < 1.6$  GeV/ $c$  and  $p_T > 1.1$  GeV/ $c$ . The results are shown in fig. 2 for the two  $p_T$  ranges. At low  $p_T$  (fig. 2, left), the NA60 In-In data show an increase with  $N_{part}$ , in agreement with the NA49 results in the same range. At high  $p_T$  (fig. 2, right) a flattening of the inverse slope dependence on centrality is observed, analogously to the NA50 results. However, while the difference between the low- $p_T$  NA49 results and the high- $p_T$  NA50 results

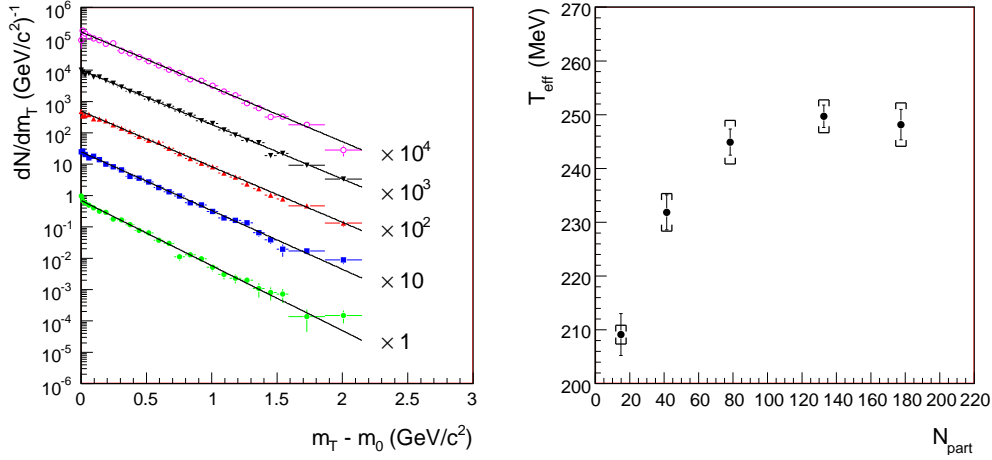


**Figure 1.** Left panel:  $\phi$  transverse momentum distributions in indium-indium collisions as a function of centrality. From top to bottom: central to peripheral spectra. Right Panel:  $T$  slope parameter as a function of the number of participants.

amounts to  $\sim 70$  MeV for central collisions, the same difference in the NA60 In-In data is of  $\sim 15$  MeV. While the latter can presumably be due to radial flow, the magnitude of the effect in Pb-Pb can hardly be attributed entirely to the same cause. A further flattening due to kaon rescattering and absorption may lead to larger  $T_{eff}$  values in the NA49 data.

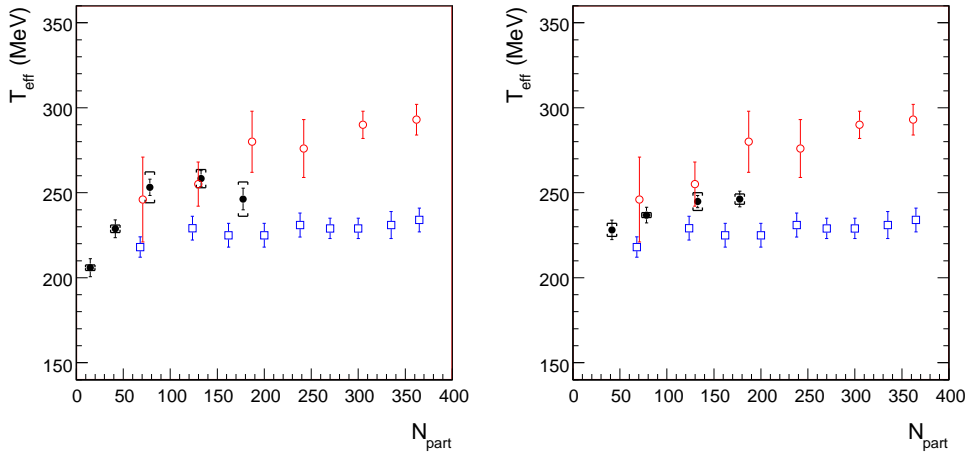


**Figure 2.** Centrality dependence of the  $T_{eff}$  slope parameter (full circles) compared to NA49 (open circles) and to NA50 (open squares). Left panel: fit performed in the NA49 range ( $0 < p_T < 1.6$  GeV/c). Right panel: fit performed in the NA50 range ( $1.1 < p_T < 3$  GeV/c).

The  $\phi$  multiplicity was obtained with two different approaches, with largely independent systematic errors. In the first, the cross section is directly measured, counting the number of  $\phi$  produced and the number of incident ions. The average  $\phi$  multiplicity is then obtained dividing the  $\phi$  cross section by the total In-In inelastic

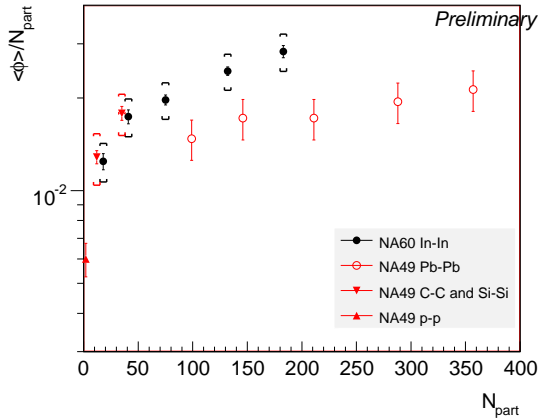


**Figure 3.**  $\langle\phi\rangle/N_{part}$  in full phase space, compared to the NA49 measurement in several collision systems.

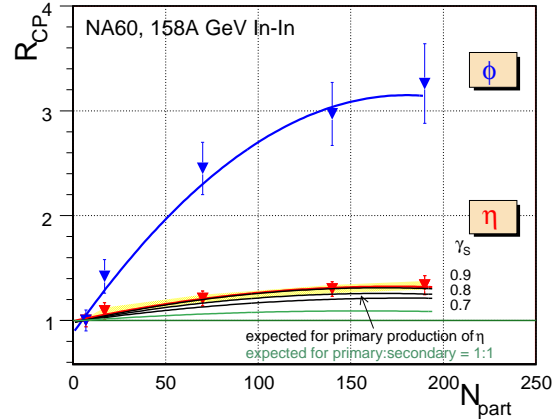


**Figure 4.**  $R_{CP}$  for the  $\eta$  compared to the one for the  $\phi$  and the expectation for primary production only.

cross section, estimated with the general formula for two nuclei of mass numbers  $A$  and  $B$ :  $\sigma_{inel,AB} = \pi r_0^2 [A^{1/3} + B^{1/3} - \beta (A^{-1/3} + B^{-1/3})]$  [11], with  $r_0 = 1.3$  and  $\beta = 1.93$  which leads to  $\sigma_{inel,In-In} = 4.32$  b. Alternatively, the  $\phi$  multiplicity can be obtained using the  $J/\psi$  as a calibration process. The ratio between the  $\phi$  and the  $J/\psi$  multiplicities is given by:  $\langle\phi\rangle/\langle J/\psi\rangle = (N_\phi/A_\phi \times \epsilon_{rec,\phi})/(N_{J/\psi}/A_{J/\psi} \times \epsilon_{rec,J/\psi})$ , where  $N_{\phi(J/\psi)}$ ,  $A_{\phi(J/\psi)}$  and  $\epsilon_{rec,\phi(J/\psi)}$  are the number of observed  $\phi$  ( $J/\psi$ ) resonances, the acceptance and the reconstruction efficiency respectively. Once corrected for anomalous and nuclear absorption,  $\langle J/\psi\rangle$  scales with the number of binary collisions  $N_{coll}$  and can be written as  $\langle J/\psi\rangle = (\sigma_{NN}^{J/\psi}/\sigma_{NN}) \cdot N_{coll}$ , where  $\sigma_{NN}^{J/\psi}$  and  $\sigma_{NN}$  are the  $J/\psi$  and inelastic cross sections in nucleon-nucleon collisions, and  $N_{coll}$  is calculated from  $N_{part}$  using the Glauber model. By multiplying this value by the above ratio, one obtains  $\langle\phi\rangle$ . The two methods agree within  $\sim 10\%$ .

In fig.3 the  $\phi$  enhancement factor, expressed as the ratio  $\langle\phi\rangle/N_{part}$  is plotted as a function of  $N_{part}$ , compared to the NA49 results in several collision systems [12], [9]. The value in central In-In collisions exceeds the corresponding NA49 one in Pb-Pb. A direct comparison with NA50 requires an extrapolation of the NA50 measurements to low  $p_T$ , and is difficult due to the discrepancies in the observed inverse slopes. Two extreme cases with  $T_{eff} = 220$  MeV and  $T_{eff} = 300$  MeV were considered. The corresponding results largely exceed the NA60 values even if the higher  $T_{eff}$  value is considered.

To conclude, the  $\phi$  puzzle is not yet solved. The forthcoming NA60 measurement in the  $\phi \rightarrow KK$  channel may be decisive to clarify the picture.

#### 4. $\eta$ enhancement

The  $\eta$  meson, carrying a strangeness content of  $\sim 40\%$ , is expected to be strangeness-enhanced in heavy ion collisions. NA60 detects the  $\eta$  through its Dalitz decay  $\eta \rightarrow \mu\mu\gamma$ .

In fig. 4 the  $R_{CP}$  of the  $\eta$ , defined as  $R_{CP}^\eta(N_{part}) = \langle \eta \rangle / N_{part} / [\langle \eta \rangle / N_{part}]_{peripheral}$ , is plotted as a function of  $N_{part}$ , compared to the  $\phi$ . An enhancement of the  $\eta$  by a factor 1.34 from most peripheral to most central collisions is observed. The values for the  $\eta$  and  $\phi$  mesons can be linked through the strangeness under-saturation parameter  $\gamma_s$ . According to [13], the value of  $\gamma_s$  is  $\sim 0.7$  in Si-Si and  $\sim 0.9$  in Pb-Pb central collisions. A value of 0.8 in central In-In collisions is assumed. Since  $\phi$  is produced only primarily, the dependence on centrality of  $\gamma_s$  can be then extracted from the  $\phi$   $R_{CP}$ , according to the scaling:  $\langle \phi \rangle / N_{part1} / \langle \phi \rangle / N_{part2} = \gamma_s^2(N_{part1}) / \gamma_s^2(N_{part2})$ . The  $\eta$   $R_{CP}$  can then be calculated under the hypothesis that  $\eta$  is only primary produced: in this case  $\eta / N_{part} \propto 0.4\gamma_s^2(N_{part}) + 0.6$ . The result of the calculation is plotted in fig. 4, assuming values for  $\gamma_s$  that range from 0.7 to 0.9 in central collisions. It should be noted that the results agree with the expectations if only primary production is assumed, in contrast to Statistical Models where a large fraction of the  $\eta$  is produced from secondaries without strangeness [14]. For comparison, if the ratio between primary and secondary production (the latter coming mainly from the decays of  $\pi_1(1400)$  and  $a_0$  which are not  $\gamma_s$  suppressed) would be 1:1, the expected enhancement from peripheral to central collisions would be  $\sim 1.1$ .

## 5. Results in the intermediate mass region

The dimuon intermediate mass region (IMR), located between the  $\phi$  and the  $J/\psi$  peaks, is expected to be well suited for the search of thermal dimuons, due to its relative production yield with respect to the other expected contributions in this region. In p-A collisions, the IMR region is described as a superposition of the Drell-Yan and open charm sources [15]. The NA38, NA50 and HELIOS-3 experiments observed an excess in the IMR with respect to the extrapolation of these sources in S-U and Pb-Pb collisions [15], [16]. The mass spectrum of the excess has the same shape as the open charm. Possible explanations of this excess are the production of thermal dimuons or the enhancement of the charm cross section. In the former case, the excess would have a prompt origin, while in the latter the muons coming from charmed meson decays would be off-vertex. Due to limited vertex capabilities, it was not possible to distinguish between the two scenarios.

Thanks to its ability to measure the muon offset, NA60 can distinguish, on a statistical basis, between prompt and off-vertex dimuons. The resolution of the offset distance between the muon tracks and the vertex, estimated using muon pairs from  $J/\psi$  decay, is  $37 \mu\text{m}$  in the x coordinate (bending plane) and  $45 \mu\text{m}$  in y. Since the offset resolution of the matched tracks is affected by multiple scattering and energy loss, a weighted offset is used in the analysis:  $\Delta_\mu = \sqrt{\Delta x^2 V_{xx}^{-1} + \Delta y^2 V_{yy}^{-1} + 2\Delta x \Delta y V_{xy}^{-1}}$  where  $V^{-1}$  is the inverse error matrix, accounting for the uncertainties of the vertex fit and of the muon kinematics,  $\Delta x$  and  $\Delta y$  are the differences between the vertex coordinates and those of the extrapolated muon track at  $z = z_{vert}$ . The dimuon offset is defined as  $\Delta_{\mu\mu} = \sqrt{(\Delta_{\mu1}^2 + \Delta_{\mu2}^2)/2}$ .

NA60 observes an excess in the mass region  $1.16 < M < 2.56 \text{ GeV}/c^2$  with respect to the expected sources, that increases from peripheral to central collision faster than  $N_{part}$  and Drell-Yan.

The dimuon offset distribution, shown in fig.5 for  $1.16 < M < 2.56 \text{ GeV}/c^2$ , is compared to the corresponding distributions for prompt dimuons and open charm, scaled with respect to extrapolations from p-A data. It can be noticed that, in order to describe the data, the prompt dimuon source must be scaled by a factor 2.43 with respect to the expected Drell-Yan, while no enhancement is observed for the open charm, within errors. Therefore, the excess can be ascribed to a prompt source.

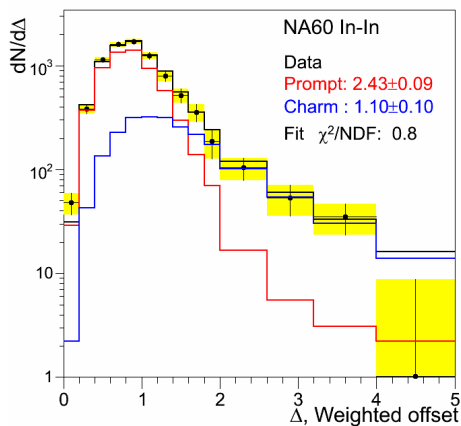


**Figure 5.** Dimuon weighted offset compared to the superposition of Drell-Yan and open charm contributions.

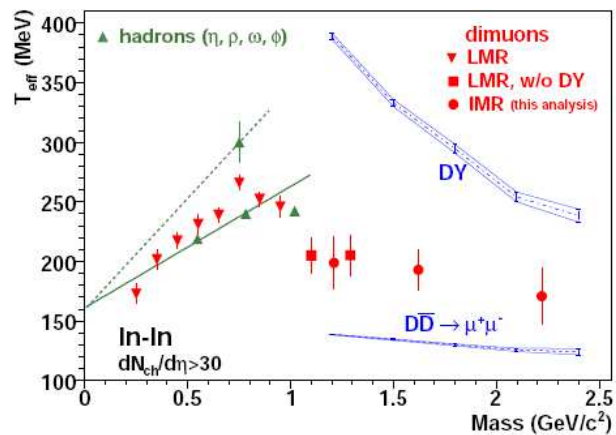


**Figure 6.** Inverse slope parameter versus dimuon mass. For details, see [17].

In order to study the properties of the excess, the expected Drell-Yan and open charm contributions were subtracted to the data. The resulting excess mass distribution is not reproduced by the Drell-Yan process, being much flatter. The  $p_T$  spectrum of the excess is significantly softer than the Drell-Yan one. Moreover, the excess  $p_T$  spectra extracted from different mass windows in the IMR are clearly different, while for the Drell-Yan pairs mass and  $p_T$  spectra factorize, and are thus independent. More details on the analysis and results are reported in [3]. The properties of the observed prompt excess, being different from the Drell-Yan ones in many observables, suggest an interpretation as thermal radiation.

The inverse  $m_T$  slope extracted for three mass windows in the IMR, is plotted in fig. 6 as a function of the mass, together with the corresponding values obtained in the low mass region [17]. The inverse slopes for the Drell-Yan and open charm contributions are shown for comparison. Below  $1 \text{ GeV}/c^2$ , the inverse slope parameters monotonically rise with mass from the dimuon threshold where  $T \sim 180 \text{ MeV}$ , up to the nominal pole of the  $\rho$  meson, where  $T \sim 250 \text{ MeV}$ . This is followed by a sudden decline to  $\sim 190 \text{ MeV}$  in the IMR. The initial rise is consistent with the expectation for radial flow

of a hadronic source (here  $\pi^+\pi^- \rightarrow \rho \rightarrow \mu\mu$ ). The jump of  $\sim 50$  MeV observed beyond  $1 \text{ GeV}/c^2$ , down to a low-flow situation, is extremely hard to reconcile with emission sources which continue to be of dominantly hadronic origin. Rather, the sudden loss of flow is most naturally explained as a transition to a qualitatively different source, implying dominantly early, i.e. partonic processes like  $q\bar{q} \rightarrow \mu\mu$ , for which flow has not yet built up.

## 6. Summary

The NA60 experiment measured dimuon production in In-In collisions at the CERN SPS. The  $\phi$  yield observed in the leptonic channel is higher than the one observed by NA49 in the hadronic channel in Pb-Pb collisions. The dependence of the inverse slope on  $p_T$  suggests that the difference between NA49 and NA50 is larger than expected from radial flow. The forthcoming NA60 measurement in the  $\phi \rightarrow KK$  channel may be decisive to clarify the picture.

The  $\eta$  meson shows an enhancement of a factor 1.34 from peripheral to central collisions. This enhancement, compared to the  $\phi$  one, is consistent with the expectation in the hypothesis that the  $\eta$  is only primarily produced.

In the intermediate mass region, an excess of prompt origin is observed. The Drell-Yan process can not reproduce the properties of the excess. The value of  $T_{eff}$ , significantly smaller than in the low mass region, suggests an emission from the partonic stage, when the transverse flow has not yet built up.

## References

- [1] J. Rafelski and B. Muller, Phys. Rev. Lett. 48 (1982) 1066.
- [2] E. V. Shuryak, Phys. Rep. 61 (1980) 71.
- [3] R. Arnaldi et al. (NA60 Coll.) Eur. Phys. J. C (2009) in press. arXiv:0810.3204.
- [4] B. Alessandro et. al. (NA50 Coll.), Phys. Lett. B 555 (2003) 147.
- [5] S. V. Afanasev et. al. (NA49 Coll.), Phys. Lett. B 491 (2000) 59.
- [6] E.V. Shuryak, Nucl. Phys. A661 (1999) 119; Johnson S C, Jacak B V and Drees A, Eur. Phys. J. C18 (2001) 645; Pal S, Ko C M and Lin Z, Nucl. Phys. A707 (2002) 525
- [7] D. Adamova et. al. (CERES Coll.), Phys. Rev. Lett. 96 (2006) 152301.
- [8] M. Floris et. al. (NA60 Coll.), J. Phys. G 35 (2008) 104054.
- [9] C. Alt et al. (NA49 Coll.), Phys. Rev. Lett. 94 (2005) 052301;
- [10] C. Amsler et. al. (Particle Data Group), Phys. Lett. B 667 (2008) 1.
- [11] M.Kh. Anikina et. al., Soviet Journal of Nuclear Physics, Yad. Fiz 38 (1983) 88
- [12] V. Friese et al. (NA49 Coll.), Nucl. Phys A 698 (2002) 487; C. Alt et al. (NA49 Coll.), Phys. Rev. C 73 (2006) 044910;
- [13] F. Becattini et al., Phys.Rev.C 73 (2006) 044905
- [14] F. Becattini, private communication.
- [15] M.C. Abreu et al. (NA50 Coll.) Eur. Phys. J. C14 (2000) 443
- [16] C. Lourenco et al., Nucl. Phys. A566 (1994) 77; A.L.S. Angelis, Eur. Phys. J C13 (2000) 433.
- [17] R. Arnaldi et al. (NA60 Coll.), Phys. Rev. Lett. 100 (2008) 022032